Open access • Journal Article • DOI:10.1111/CLR.13019

Quantitative evaluation of metal artifacts using different CBCT devices, high-density materials and field of views. — Source link

Marina Codari, Karla de Faria Vasconcelos, Laura Ferreira Pinheiro Nicolielo, Francisco Haiter Neto ...+1 more authors

Institutions: Katholieke Universiteit Leuven, State University of Campinas

Published on: 22 Apr 2017 - Clinical Oral Implants Research (Clin Oral Implants Res)

CLINICAL ORAL IMPLANTS RESEARCH

Marina Codari
Karla de Faria Vasconcelos
Laura Ferreira Pinheiro Nicolielo
Francisco Haiter Neto
Reinhilde Jacobs

Quantitative evaluation of metal artifacts using different CBCT devices, high-density materials and field of views

Authors' affiliations:
Marina Codari, Karla de Faria Vasconcelos, Laura Ferreira Pinheiro Nicolielo, Reinhilde Jacobs, OIC, OMFS IMPATH Research Group, Department Imaging & Pathology, Faculty of Medicine, KU Leuven and Oral and Maxillofacial Surgery, University Hospitals Leuven, Leuven, Belgium
Marina Codari, Department of Biomedical Sciences for Health, Faculty of Medicine and Surgery, Università degli Studi di Milano, Milano, Italy
Karla de Faria Vasconcelos, Francisco Haiter Neto, Division of Oral Radiology, Department of Oral Diagnosis, Piracicaba Dental School, State University of Campinas, Piracicaba, São Paulo, Brazil

Corresponding author:
Marina Codari, MSc, PhD
Department of Biomedical Sciences for Health
Faculty of Medicine and Surgery, Università degli Studi di Milano
Via Mangiagalli 31, 20133, Milano, Italy
Tel.: +39 02 503 15390
Fax: +39 02 503 15387
e-mail: marina.codari@unimi.it

Key words: artifacts, cone-beam computed tomography, density materials, field of view

Abstract

Objective: To objectively compare the influence of different cone-beam computed tomography (CBCT) devices, high-density materials and field of views (FOVs) on metal artifact expression.

Material and methods: For this *in vitro* study, three customized acrylic resin phantoms containing high-density materials cylinders: titanium, copper–aluminum alloy and amalgam were scanned on three CBCT devices using high-resolution protocols, same voxel size (0.2 mm) and different FOVs. After fully automatic segmentation and image registration, the same region of interest was defined for the small and medium FOVs. The difference between the segmented and the real volume of the metal cylinders was assessed. Moreover for each segmented slice, the area difference between the segmented and the real axial section was determined. The artifacts on the background were measured as normalizing standard deviation of voxel values in the vicinity of the cylinder, in three different distances.

Results: Considerable differences were observed in volume measurements for all CBCTs devices and materials for both FOV sizes (up to 67%). The slice per slice area analysis indicated higher artifacts at the edges of the metal cylinder. Within the materials, amalgam and titanium had, respectively, the worst and best artifact expression in all the CBCT devices. Standard deviation values varied differently between the three distances in each device.

Conclusion: Our *in vitro* study showed that different CBCT devices, high-density materials and FOV should be considered while evaluating CBCT images. More carefully, diagnosis conclusions should be drawn in images containing amalgam and copper–aluminum alloy.

Since the advent of cone-beam computed tomography (CBCT), attempts to quantify image artifacts have gained importance. For this reason, in the last few years, research focused on the evaluation of the factors that influence artifact expression in CBCT images in order to better understand how to analyze and improve corrupted images (Benic et al. 2013; Kuusisto et al. 2015; Sancho-Puchades et al. 2015).

Artifacts can be seen in the reconstructed images and several etiologies have been reported in the literature (Schulze et al. 2011; Pauwels et al. 2013). Among the possible causes of artifacts, beam hardening is described as the most common, followed by the noise, nonlinear partial volume effect, motion and scatter (De Man et al. 1999).

One of the main causes of artifacts is the presence of high-density materials within the field of view (FOV), such as metal implants, intracanal posts, metallic crowns and amalgam restoration. The literature has demonstrated that metal artifacts have negative influence in the daily diagnosis. In particular, their presence influences root fracture diagnosis in CBCT images in the presence of intracanal materials and metal posts (Hassan et al. 2010; Melo et al. 2010; Costa et al. 2011, 2012; da Silveira et al. 2013). This negative influence is caused by the appearance of dark streak artifacts mimicking the fracture lines disturbing the diagnostic process, leading to an incorrect diagnosis and treatment plan and in some cases to unnecessary extraction.

Similar limitations may occur when looking to dental implant surfaces and their bony coverage. Despite the CBCT provide accurate information related to bone morphology and guidance on the positioning of the implant in the alveolar ridge (Guerrero et al. 2006), the

Date:
Accepted 14 March 2017

To cite this article:
Codari M, De Faria Vasconcelos K, Ferreira Pinheiro Nicolielo L, Haiter Neto F, Jacobs R. Quantitative evaluation of metal artifacts using different CBCT devices, high-density materials and field of views.
Clin. Oral Impl. Res. **00**, 2017, 1–6
doi: 10.1111/clr.13019

peri-implant region can be compromised by the presence screw artifacts hindering or even making impossible the diagnosis in this region (Kamburoğlu et al. 2013; Sancho-Puchades et al. 2015). The latter may surely apply when imaging multiple implants and the prosthetic superstructure in one jaw.

High-density materials can create artifacts that affect image quality in different ways depending on the CBCT device (Vasconcelos et al. 2015) and imaging protocol. For this reason, acquisition parameters, detector type and reconstruction algorithms are important parameters that must be taken into account while evaluating image quality in terms of image noise, contrast resolution and artifacts (Goldman 2007).

Given the influence of such factors on artifact generation and in order to better understand their expression in CBCT images, the aim of the present research was to evaluate the influence of different CBCT devices, materials and FOV sizes on metal artifact generation.

Material and methods

Phantoms

For this study, three acrylic resin (VIP, São Paulo, Brazil) phantoms with 98 mm of diameter × 40 mm of height were manufactured. Each phantom contained three 5 × 5 mm cylindrical pins made with different high-density materials: titanium, copper–aluminum alloy (CuAl) and amalgam. These cylinders were positioned at the vertices of an isosceles triangle to mimic the position of the central incisors (A) and second molars (B and C) in a human mandible. Phantom geometry and composition is described in Fig. 1.

The dimensions of the metallic cylinders were checked with a digital sliding calliper (0–150 mm Stainless, Hardened®) before their inclusion in the resin phantom. Moreover, their correct position inside the phantom was certified using a comparative microscope (Olympus Optical CO, LTD, Japan), to standardize the geometry of all phantoms.

CBCT parameters

All phantoms were scanned using 0.2 mm voxel size and one representative medium and small FOV for each CBCT device: CBCT 1 – 3D Accuitomo 170 (J. Morita, Kyoto, Japan); CBCT 2 – Newtom VGI evo (Newtom, Verona, Italy) and CBCT 3 – ProMax 3D (Planmeca Oy, Helsinki, Finland). All exposure protocols are shown in Table 1.

Image analysis

During image analysis, for each combination of CBCT device and material, the images acquired with medium and small FOV were simultaneously analyzed.

As first image processing step, the automatic segmentation of metal cylinders in both images was performed, thus allowing to quantify the effect of metal artifact. Segmentation was based on three-dimensional *k*-means clustering approach (Hartigan & Wong 1979), with all voxels classified in three categories (air, acrylic resin and metal). Then, the voxels belonging to the most intense cluster were classified as metal.

After the segmentation, to select the same region of interest (ROI) in both small and medium FOV images, these two images were registered. In particular, small FOV images were chosen as moving image, while the medium FOV images were selected as reference images. This step was performed automatically and was divided into two substeps. The first registration substep consisted of the estimation of the initial translation transformation that allowed to roughly register each pair of volumes. This step was performed automatically detecting the metal cylinders in B position, which were present in both FOVs, to calculate their barycenter and estimate the initial rigid transformation. After this initialization step, a fine intensity-based registration method was used to register each pair of volumes. For this registration step, the normalized mutual information was applied as registration metric (Hill et al. 2001).

Once each pair of volumes was registered, the same ROI could be selected. This ROI was automatically defined as the portion of the acrylic resin phantom that was imaged in both FOVs. All the acquired images were analyzed using MATLAB (MathWorks, Natick, USA). The flowchart of the described image processing is depicted in Fig. 2.

Within the selected ROIs, to evaluate how the metal cylinder geometry was corrupted by metal artifacts, the volume difference between the segmented volume, obtained as outcome of the image processing steps, and the real volume, geometrically calculated knowing the dimensions of cylinder diameter (5 mm) and height (5 mm), was calculated. This volume difference (V_D) was expressed as percentage of the real volume of the metal cylinder. Moreover, the difference between the segmented and real area (A_D) was evaluated in each axial slice.

To evaluate the impact of the metal artifact in the surrounding voxels, the voxels segmented as metal were removed from the ROI. Once removed, the new ROI was divided into three sub-ROIs. In this way, the amount of artifacts was evaluated taking into account the distance between the surrounding voxels and the metal object. Figure 3 shows an example of ROI division.

Finally, to quantify the amount of artifacts in these regions, we calculated the normalized standard deviation (nSD), defined as:

$$\mathrm{nSD} = \frac{\mathrm{SD_s}}{2^{(\text{stored bits}-1)}}$$

where SD_s represent the SD value of the surrounding voxels, which was subsequently divided by the maximum possible SD value (Pauwels et al. 2013). The SD of the voxels contained in the ROI was normalized to the maximum possible SD value, defined as half or the full gray value range, which allowed us to compare different CBCT devices with different gray value ranges. As the phantom is homogeneous, in an ideal condition, the surrounding voxels should have the same intensity value and, consequently, a nSD value equal to 0%. On the other hand, in the real condition, due to the presence of metal artifacts, this value will diverge from 0% proportionally to the amount of artifacts. For this reason, nSD was chosen as metric for image quality quantification in surrounding voxels near to the metal object.

Statistical analysis

Data were analyzed with a three-way ANOVA model, with CBCT device, material and FOV as three crossed factors. As there was only one measurement for each combination for volume, area and nSD measurements of the different ROIs, a solution was found by leaving out the interaction factor if the three main factors were out of the model, and hence considering only the main factors and each of the interaction factors of the main factor. Any difference between measured values that may point to a three-way interaction was explained by experimental error. Level of statistical significance was set for a P-value <0.05.

Results

Differences between segmented and real volume were observed for all CBCT devices and materials. Results of V_D analysis are shown in Table 2. Statistical differences were found among different materials for different combination of CBCT devices and FOVs ($P < 0.05$).

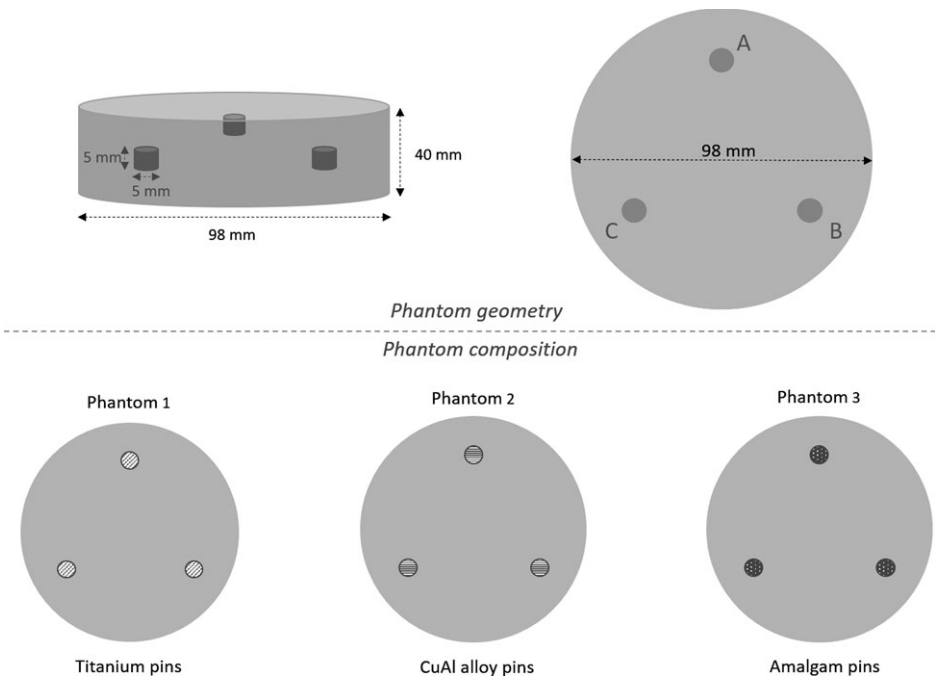

Fig. 1. Geometry and composition of the three phantoms used in this study.

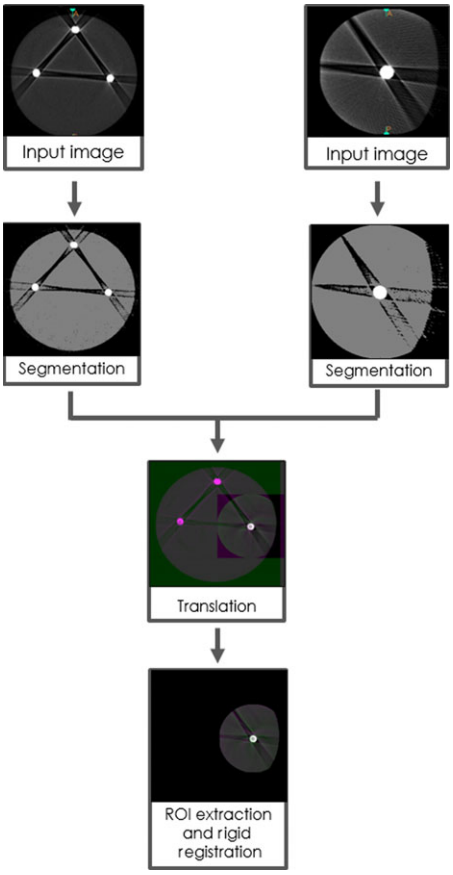

Fig. 2. Flowchart of the image processing process used to extract the same ROI from the images obtained for each combination of CBCT device, material and FOV.

Table 1. **Exposure protocols for CBCT devices**

	ID	FOVs (cm)	kVp	mA	Exposure time (s)	Voxel size (mm)
3D Accuitomo 170	CBCT 1	4.0 × 4.0/10.0 × 5.0	90.0	5.0	30.8/17.5	0.2
Newtom VGI evo	CBCT 2	5.0 × 5.0/10.0 × 5.0	110.0	3.0	1.8/1.8	0.2
ProMax 3D	CBCT 3	5.0 × 5.0/10.0 × 5.0	96.0	5.6	12.0/12.0	0.2

Moreover, statistical significant differences were found in volume measurements varying CBCT devices ($P < 0.05$), but not varying FOV size ($P > 0.05$). Figure 4 shows the difference between segmentation for each combination of CBCT device, material and FOV.

For A_D, significant difference was observed for all combinations of FOV, CBCT device and material. The results of this analysis are summarized in Table 3.

Normalized standard deviation varied differently between the three ROIs in each device (Table 4). There was no significant difference between materials for all combinations of CBCT and FOV ($P > 0.05$). Only CBCT3 showed significant difference in nSD values for all combinations of FOV and materials ($P < 0.05$). Finally, the small FOV in all the CBCT devices showed statistical significant differences ($P < 0.05$).

Discussion

The present study showed the influence of different high-density materials, CBCT devices and FOVs on the image quality, using a novel and fully objective method.

In CBCT images, gray values' intensity is specific for each equipment due to the influence of technique factors inherent for each device. Usually, in modern CBCT devices, the acquired images are stored as 12-bit or 16-bit DICOM images. Difference in the number of stored bits lead to a different number of possible gray values, which is defined as $2^{(\text{stored bit})}$. To compensate these differences and be able to compare SD values from different CBCT devices without any other a priori information on image histogram content, nSD was calculated (Pauwels et al. 2013).

Independently of this specific characteristic related to each CBCT device, the presence of high-density materials produce severe artifacts in the reconstructed data. These artifacts are even worse when these materials are present in more than one place inside scanning geometry. In this case, the region between two such objects is deteriorated, impairing radiodiagnosis. Such artifacts are denoted with a variety of terms. Some of them are called "missing value artifacts" (Schulze et al. 2011) while others refer to "photon starvation" (Scarfe & Farman 2008; Molteni 2013; Yuan et al. 2016). It is a very common artifact generated by the beam-hardening phenomenon resulting in dark bands or "photon starvation" between dense objects and cupping artifacts (Molteni 2013) and is a "hot" topic in current radiology research.

In the present study, both artifacts were observed in all the samples for all the materials reducing the image quality. Several studies demonstrated that CBCT image quality can be improved by changing some parameters during scanning procedure, such as kVp (Draenert et al. 2007; Chindasombatjaroen et al. 2011; Esmaeili et al. 2012; Helvacioglu-Yigit et al. 2016), mA (Pauwels et al. 2015), FOV (Pauwels et al. 2016) and voxel size (Spin-Neto et al. 2013). Therefore, in the present study, the protocols for each CBCT were carefully established. A fixed voxel size was selected to eliminate partial volume artifacts, standardizing image quality analysis. However, even choosing similar protocols, results showed statistical differences in volume measurements among CBCT devices. In particular, CBCT1 and CBCT2 seemed to have the same behavior for all combination of material and FOV ($P > 0.05$), while CBCT3 showed

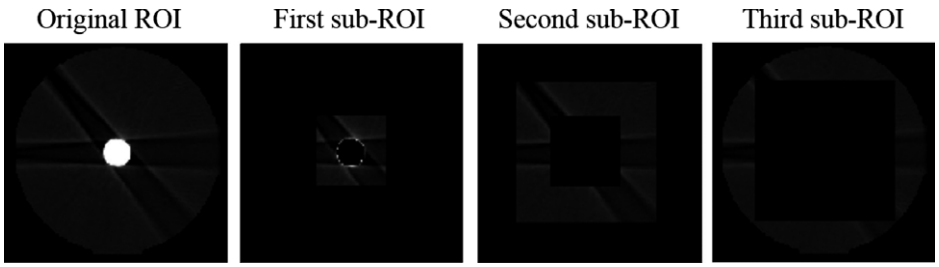

Fig. 3. Different region of interest created around the metal object and used to evaluate artifact expression.

Table 2. **V_D values (%) for all the combinations of CBCT device, material and FOV**

	CBCT 1	CBCT 2	CBCT 3
Titanium			
MFOV	3.7	2.1	23.1
sFOV	1.7	0.2	22.3
CuAl			
MFOV	−6.0	−2.6	27.9
sFOV	−7.1	−5.4	25.3
Amalgam			
MFOV	12.3	15.7	67.0
sFOV	8.6	13.8	60.2

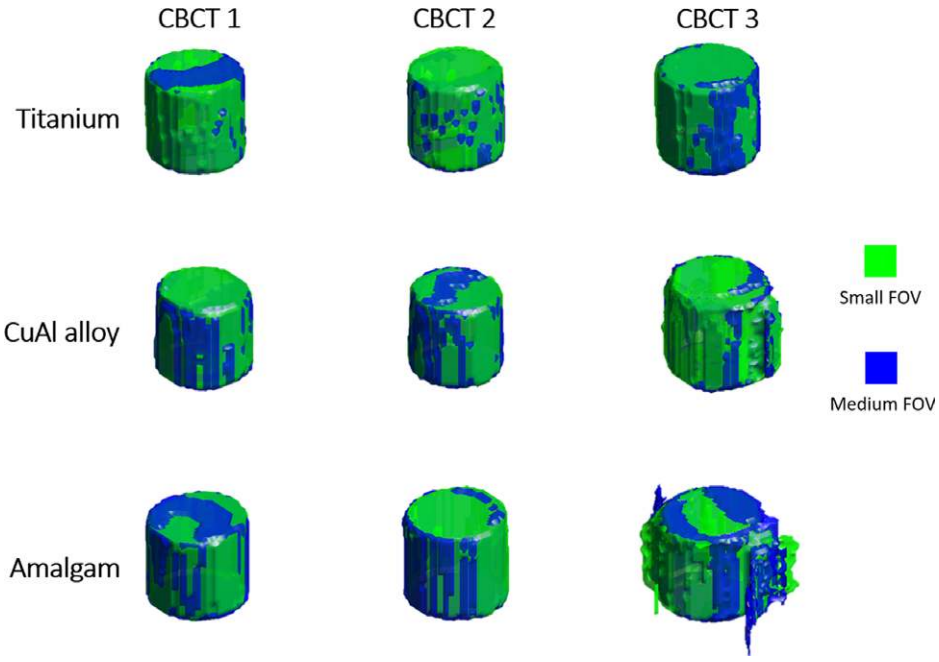

Fig. 4. Three-dimensional volume rendering of the metal cylinder segmented in all the images used for this study.

Table 3. **Median and interquartile range of A_D values (%), for all the combination of CBCT device, material and FOV**

	CBCT 1	CBCT 2	CBCT 3
Titanium			
MFOV	4.4 (0.6)	3.0 (1.5)	17.5 (0.6)
sFOV	3.3 (0.8)	1.9 (1.3)	17.1 (1.1)
CuAl			
MFOV	−0.8 (3.5)	0.6 (3.5)	23 (7.5)
sFOV	−2.2 (4.7)	−1.4 (4.8)	23.6 (7.7)
Amalgam			
MFOV	13.6 (3)	16.0 (1.4)	61.5 (15.5)
sFOV	11.2 (1.1)	14.0 (2.1)	53.6 (10.4)

significant differences compared to the other devices ($P < 0.05$). This behavior can be explained by the differences in operating characteristics of each X-ray tube. The latter varies with different voltage peaks and therefore, different effective beam energies.

Despite of choosing similar protocols, the presence of high-density material in the scanned volume led to severe artifacts. In dentistry, a number of dense materials are currently in use, which can differ in density and uniformity. In this study, we used three different materials to evaluate the effect of their proprieties on metal artifact generation. In particular, amalgam, which is a heterogeneous material composed by mercury ($Z = 80$), silver ($Z = 47$), tin ($Z = 50$) and zinc ($Z = 30$), showed a different behavior compared to CuAl (Copper $Z = 39$ and Aluminum $Z = 13$) and Titanium ($Z = 22$). The high density of this material compared to the others causes strong artifacts that lead to high volume overestimation during segmentation.

In this study, segmented volume analysis allows to globally evaluate the effect of metal artifact on metal cylinder segmentation. On the other hand, the area analysis allowed to evaluate slice by slice if the over- or underestimation was constant through the metal object.

Our findings showed that amalgam had the highest values of median area overestimation and interquartile range (IQR). In particular, the high value of median overestimation can be due to the high density of the material that causes strong artifacts. In the same way, the high IQR values can be related to its heterogeneity that causes a large variability in A_D values on different slices. This hypothesis is then confirmed by the values measured in titanium cylinders, which is a homogenous material with a lower atomic number that showed the lowest values for both median and IQR of A_D values. These results allow us to correlate the effect of metal artifact not only to material density but also to their homogeneity.

Moreover, the area analysis allowed to observe that the segmentation of the metal object was mainly affected in the initial and final slices of the metal cylinders. This behavior was common for all samples, highlighting the strong effect of artifacts at the vertical edges of the metal object. Probably, this can be explained by the divergence of the vertical beam in the extremes. The beam diverges from the ideal perpendicularity to the rotation axis and the detector. According to Molteni (2013), a slight but consistent

Table 4. **nSD values (%) for all the combinations of CBCT device, material, FOV and sub-ROI**

	CBCT1						CBCT2						CBCT3					
	Amalgam		CuAl		Titanium		Amalgam		CuAl		Titanium		Amalgam		CuAl		Titanium	
	MFOV	sFOV	MFOV	sFOV	MFOV	sFOV	MFOV	sFOV	MFOV	sFOV	MFOV	sFOV	MFOV	sFOV	MFOV	sFOV	MFOV	sFOV
ROI 1	2	2.7	1.8	2.2	1.1	1.4	1.6	1.7	1.3	1.4	0.9	0.9	15.1	13.9	12.4	11.2	6.3	6.3
ROI 2	0.5	0.7	0.4	0.6	0.2	0.5	0.4	0.5	0.3	0.3	0.1	0.1	6.0	5.0	4.6	3.9	2.7	2.2
ROI 3	0.5	2.2	0.5	1.7	0.5	1.3	0.6	0.7	0.5	0.5	0.4	0.5	7.9	7.3	7.7	7.2	7.6	6.9
Total	0.6	1.9	0.6	1.5	0.5	1.3	0.6	0.8	0.5	0.6	0.4	0.4	8.1	7.4	7.5	6.9	6.6	6.1

increase in gray values intensity can be noticed moving toward the top. Moreover, the inaccuracy of area segmentation at the edges of the metal cylinder can be also explained considering the fact that even a very slight tilt of the phantom could lead to deviations at the edge of the object, making the axial slice not to be cutting through the entire object anymore. To reduce this source of inaccuracy, in future studies, the few slices can be removed at cylinder extremities before making the analysis.

Currently in literature, there are no articles published that quantitatively evaluate volume overestimation varying device, material and FOVs. The quantification of inaccuracy in metal object volume and area quantification can be of help for clinician during the evaluation of corrupted images, making them more aware of the amount of volume difference between the real object and the one imaged in the CBCT data.

Regarding the amount of background artifacts, quantified using nSD, there was no significant difference in nSD values between materials for all combinations of CBCT and FOV ($P > 0.05$), proving that the difference among material affects more metal segmentation than background artifacts. Moreover, our results confirmed that amalgam, compared to the other two materials, increased the SD of surrounding voxel intensity. This finding is in line with a recent study comparing SD values of intensity values in metal artifacts generated by amalgam and composites (Helvacioglu-Yigit et al. 2016).

The results of the present study showed also a significant difference between the three analyzed CBCTs, but only in the small FOV. In particular, in the third sub-ROI of small FOV images acquired with CBCT 1, we observed an increased value of nSD caused by the concomitant presence of truncation, halation artifacts (usually present in the periphery of FOV) and metal artifacts.

At the same time, the presence of few artifacts in medium FOV images, may be explained by the scattered radiation and differences related to the scanning process (i.e., scanning geometry and image reconstruction and preprocessing). To reconstruct the images, those CBCT devices used different amounts of projections. For CBCTs 1 and 2, there was a 360° rotation with approximately 525 and 360 frames, respectively, while for CBCT 3 there was a 210° rotation with approximately 300 frames, generating less information for the data reconstruction. A reduced data sample leads to misregistration, sharper edges and noisier images, because of aliasing, where fine striations appear (Scarfe & Farman 2008).

The present study applies an innovative approach to assess the characteristic CBCT-related artifact expressions. We objectively evaluated how metal cylinder geometry was corrupted by metal artifacts, as well as how these artifacts had an impact on background image quality. Most of the published articles on CBCT related to metal artifacts use subjective analysis, while the present approach allowed true quantification and comparison to the gold standard. Therefore, this kind of *in vitro* study is an important step to understand more about the behavior of the metal artifacts in CBCT and help avoiding bias on subjective analysis and assist in developing tools for artifact correction.

Conclusion

Our *in vitro* results showed that different CBCT devices, high-density materials and technical factors should be considered as being responsible for a variety of artifact expressions. In clinical practice, it should be emphasized that a more careful diagnosis is necessary with conservative conclusions when materials such as amalgam and CuAl alloy are present in the scanned volume.

Acknowledgements: We are grateful to the São Paulo Research Foundation (FAPESP, Brazil) for the financial support (protocol # 2014/17744-5). In addition, we would like to thank the NEODENT Company (Curitiba, Paraná, Brazil) for providing the titanium cylinders for the present research (protocol # 0309/14).

Conflict of interest

The authors declare no conflict of interests.

References

Benic, G.I., Sancho-Puchades, M., Jung, R.E., Deyhle, H. & Hämmerle, C.H. (2013) In vitro assessment of artifacts induced by titanium dental implants in cone beam computed tomography. *Clinical Oral Implants Research* **24**: 378–383.

Chindasombatjaroen, J., Kakimoto, N., Murakami, S., Maeda, Y. & Furukawa, S. (2011) Quantitative analysis of metallic artifacts caused by dental metals: comparison of cone-beam and multi-detector row CT scanners. *Oral Radiology* **27**: 114–120.

Costa, F.F., Gaia, B.F., Umetsubo, O.S. & Cavalcanti, M.G.P. (2011) Detection of horizontal root fracture with small-volume cone-beam computed tomography in the presence and absence of intracanal metallic post. *Journal of Endodontics* **37**: 1456–1459.

Costa, F.F., Gaia, B.F., Umetsubo, O.S., Pinheiro, L.R., Tortamano, I.P. & Cavalcanti, M.G.P. (2012) Use of large-volume cone-beam computed tomography in identification and localization of horizontal root fracture in the presence and absence of intracanal metallic post. *Journal of Endodontics* **38**: 856–859.

De Man, B., Nuyts, J., Dupont, P., Marchal, G. & Suetens, P. (1999) Metal streak artifacts in X-ray computed tomography: a simulation study. *IEEE Transactions on Nuclear Science* **46**: 691–696.

Draenert, F.G., Coppenrath, E., Herzog, P., Müller, S. & Mueller-Lisse, U.G. (2007) Beam hardening artefacts occur in dental implant scans with the NewTom® cone beam CT but not with the dental 4-row multidetector CT. *Dentomaxillofacial Radiology* **36**: 198–203.

Esmaeili, F., Johari, M., Haddadi, P. & Vatankhah, M. (2012) Beam hardening artifacts: comparison between two cone beam computed tomography scanners. *Journal of Dental Research, Dental Clinics, Dental Prospects* **6**: 49–53.

Goldman, L.W. (2007) Principles of CT: radiation dose and image quality. *Journal of Nuclear Medicine Technology* **35**: 213–225.

Guerrero, M.E., Jacobs, R., Loubele, M., Schutyser, F., Suetens, P. & van Steenberghe, D. (2006) State-of-the-art on cone beam CT imaging for preoperative planning of implant placement. *Clinical Oral Investigations* **10**: 1–7.

Hartigan, J.A. & Wong, M.A. (1979) Algorithm AS 136: a k-means clustering algorithm. *Journal of the Royal Statistical Society. Series C (Applied Statistics)* **28**: 100–108.

Hassan, B., Metska, M.E., Ozok, A.R., van der Stelt, P. & Wesselink, P.R. (2010) Comparison of five cone beam computed tomography systems for the detection of vertical root fractures. *Journal of Endodontics* **36**: 126–129.

Helvacioglu-Yigit, D., Kocasarac, H.D., Bechara, B. & Noujeim, M. (2016) Evaluation and reduction of artifacts generated by 4 different root-end filling materials by using multiple cone-beam computed tomography imaging settings. *Journal of Endodontics* **42**: 307–314.

Hill, D.L., Batchelor, P.G., Holden, M. & Hawkes, D.J. (2001) Medical image registration. *Physics in Medicine and Biology* **46**: R1–R45.

Kamburoğlu, K., Kolsuz, E., Murat, S., Eren, H., Yüksel, S. & Paksoy, C.S. (2013) Assessment of buccal marginal alveolar peri-implant and periodontal defects using a cone beam CT system with and without the application of metal artefact reduction mode. *Dentomaxillofacial Radiology* **42**: 20130176. doi: 10.1259/dmfr.20130176.

Kuusisto, N., Vallittu, P.K., Lassila, L.V.J. & Huumonen, S. (2015) Evaluation of intensity of artefacts in CBCT by radio-opacity of composite simulation models of implants in vitro. *Dentomaxillofacial Radiology* **44**: 20140157. doi: 10.1259/dmfr.20140157.

Melo, S.L.S., Bortoluzzi, E.A., Abreu, M., Corrêa, L.R. & Corrêa, M. (2010) Diagnostic ability of a cone-beam computed tomography scan to assess longitudinal root fractures in prosthetically treated teeth. *Journal of Endodontics* **36**: 1879–1882.

Molteni, R. (2013) Prospects and challenges of rendering tissue density in Hounsfield units for cone beam computed tomography. *Oral Surgery, Oral Medicine, Oral Pathology and Oral Radiology* **116**: 105–119.

Pauwels, R., Jacobs, R., Bogaerts, R., Bosmans, H. & Panmekiate, S. (2016) Reduction of scatter-induced image noise in cone beam computed tomography: effect of field of view size and position. *Oral Surgery, Oral Medicine, Oral Pathology and Oral Radiology* **121**: 188–195.

Pauwels, R., Seynaeve, L., Henriques, J.C.G., de Oliveira-Santos, C., Souza, P.C., Westphalen, F.H., Rubira-Bullen, I.R.F., Ribeiro-Rotta, R.F., Rockenbach, M.I.B., Haiter-Neto, F., Pittayapat, P., Bosmans, H., Bogaerts, R. & Jacobs, R. (2015) Optimization of dental CBCT exposures through mAs reduction. *Dentomaxillofacial Radiology* **44**: 20150108.

Pauwels, R., Stamatakis, H., Bosmans, H., Bogaerts, R., Jacobs, R., Horner, K. & Tsiklakis, K. (2013) Quantification of metal artifacts on cone beam computed tomography images. *Clinical Oral Implants Research* **24**: 94–99.

Sancho-Puchades, M., Hämmerle, C.H. & Benic, G.I. (2015) In vitro assessment of artifacts induced by titanium, titanium–zirconium and zirconium dioxide implants in cone-beam computed tomography. *Clinical Oral Implants Research* **26**: 1222–1228.

Scarfe, W.C. & Farman, A.G. (2008) What is cone-beam CT and how does it work? *Dental Clinics of North America* **52**: 707–730.

Schulze, R., Heil, U., Groβ, D., Bruellmann, D.D., Dranischnikow, E., Schwanecke, U. & Schoemer, E. (2011) Artefacts in CBCT: a review. *Dentomaxillofacial Radiology*. **40**: 265–273.

da Silveira, P.F., Vizzotto, M.B., Liedke, G.S., da Silveira, H.L.D., Montagner, F. & da Silveira, H.E.D. (2013) Detection of vertical root fractures by conventional radiographic examination and cone beam computed tomography – an in vitro analysis. *Dental Traumatology* **29**: 41–46.

Spin-Neto, R., Gotfredsen, E. & Wenzel, A. (2013) Impact of voxel size variation on CBCT-based diagnostic outcome in dentistry: a systematic review. *Journal of Digital Imaging* **26**: 813–820.

Vasconcelos, K.F., Nicolielo, L.F.P., Nascimento, M.C., Haiter-Neto, F., Bóscolo, F.N., Van Dessel, J., EzEldeen, M., Lambrichts, I. & Jacobs, R. (2015) Artefact expression associated with several cone-beam computed tomographic machines when imaging root filled teeth. *International Endodontic Journal* **48**: 994–1000.

Yuan, F., Chen, L., Wang, X., Wang, Y., Lyu, P. & Sun, Y. (2016) Comparative evaluation of the artefacts index of dental materials on two-dimensional cone-beam computed tomography. *Scientific Reports* **6**: 26107. doi: 10.1038/srep26107.